Title

Time-of-flight neutral particle analyzer and calibrationa)

Journal

Review of Scientific Instruments, 79(10)

ISSN

0034-6748

Authors

Harris, WS

Garate, EP

Heidbrink, WW

et al.

Publication Date

2008-10-01

DOI

10.1063/1.2955616

Time-of-flight neutral particle analyzer and calibration[a)]

W. S. Harris, E. P. Garate, W. W. Heidbrink, R. McWilliams, T. Roche, E. Trask, and Yang Zhang
Department of Physics and Astronomy, University of California, Irvine, California 92697, USA

(Presented 14 May 2008; received 6 May 2008; accepted 4 June 2008; published online 31 October 2008)

A time-of-flight diagnostic has been implemented on the Irvine field reversed configuration (IFRC) to obtain an energy distribution function from charge-exchanged neutral hydrogen. The diagnostic includes a 13 cm radius slotted disk rotating at 165 Hz in vacuum which chops the emitted neutrals at a rate of 26 kHz. *In situ* timing verification was performed with a dc xenon discharge lamp with an uncertainty less than 100 ns for a 38 μs chopping period. Energy calibration was accomplished with a singly ionized lithium source in the range of 300–1500 eV, achieving an average energy uncertainty, $\Delta E/E$, of 0.11. The diagnostic has measured neutrals in the range of 20–80 eV from the IFRC and the corresponding energy distribution function has been obtained. © *2008 American Institute of Physics.* [DOI: 10.1063/1.2955616]

I. INTRODUCTION

Neutral particle analysis (NPA) as a passive diagnostic is useful because information about the ion distribution function can be extracted and plasma pertubations are nonexistent. In particular, time of flight (TOF) has proven to be succesful in experiments where low energy (<1 keV) neutrals are of interest.[1–4] The Irvine field reversed configuration (IFRC) is a coaxial device similar to the coaxial slow source[5] that generates a plasma current containing energetic ions in the range of 20–80 eV with a temperature of a few eV. As the FRC is formed, a toroidal electric field accelerates these ions until the magnetic field reverses and the field lines close. Observation of these fast ions is necessary to verify that ions are accelerated during this process and contribute to the total plasma current. In addition, measurements of the time-resolved energy distribution function can be compared with FRC equilibrium theory.

By performing NPA on neutral charge-exchanged products, the energies of the reactants can be obtained. In the IFRC, the dominant charge-exchange reaction is $H^+ + H \rightarrow H + H^+$. It should be noted that the charge-exchange cross section ($\sim 3.5 \times 10^{-15}$ cm^2), from Sec. V, is about two orders of magnitude larger than the neutral scattering cross section ($\sim 8 \times 10^{-17}$ cm^2) indicating that the dominant neutral particles detected are charge-exchanged products. Since the energy range is lower than the usual energy for a gas stripping cell or stripping foil for energy analysis, an alternative approach is TOF, where the neutral particle energy is calculated based on the TOF within the diagnostic.[6] In past experiments,[1–4] TOF has been a successful method of detecting neutral particles with energies less than 100 eV.

Several changes have been employed in an attempt to simplify previous TOF diagnostics. The Cu–Be plate used in prior diagnostics for secondary electron emission was necessary to boost electron multiplier signals whose gains did not exceed 10^5.[1] Channel electron multipliers (CEMs), like the one in this diagnostic, have a gain larger than 10^7 allowing the Cu–Be plate to be eliminated. Therefore, the neutrals hit the CEM directly, utilizing the fact that CEMs respond to neutrals.[7] This allows the geometry to be simplified as the detector is along the same axis as the line of sight.

Another difference is that the slotted disk is driven by a radio-controlled (RC) airplane brushless motor directly in vacuum. This motor has ball bearings, which avoid the magnetic bearing motor[1,8] and associated instabilities. A turbopump has been used before,[2,3] however RC airplane motors and controllers are much more readily available and are typically 1% of the cost. This also eliminates the need for a separate motor vacuum chamber.[4]

Since the IFRC lifetime ($\sim$100 μs) is comparable to the chopping period, it is important to be able to control when the distribution function is being sampled during the plasma discharge. To accomplish this, a synchronization circuit has been developed that utilizes a reference laser similar to those employed by previous diagnostics.[2–4] Although the reference laser has been introduced for timing referencing in the past, it has not been used for synchronization.

In Sec. II, the diagnostic and its components are described along with their implementation within the IFRC. Section III describes the timing calibration using a xenon discharge lamp. Calibration with a lithium ion source is reported in Sec. IV and data from the IFRC are presented in Sec. V.

II. THE TIME-OF-FLIGHT DIAGNOSTIC

A. Design

The primary components of the TOF diagnostic are outlined in Fig. 1. Hydrogen ions undergo charge exchange with background neutral hydrogen and are accepted into the diag-

[a)]Contributed paper, published as part of the Proceedings of the 17th Topical Conference on High-Temperature Plasma Diagnostics, Albuquerque, New Mexico, May 2008.

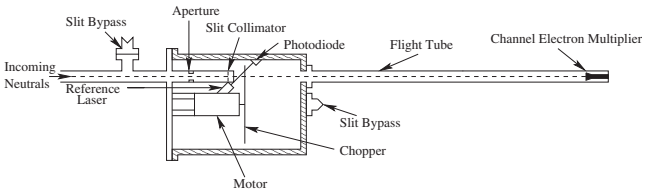

FIG. 1. Illustration of the TOF diagnostic.

nostic input flange 60 cm from the plasma center. The neutrals are then collimated by a 1 cm aperture and a single collimating slit which is 0.15 mm wide and 5 mm high. The collimated beam of neutrals then is chopped by a 13 cm radius stainless steel disk (the chopper) with 160 slits, each 0.15 mm wide, 1.5 cm long, and centered at an 11.5 cm radius. The chopper rotates at 165 Hz, giving a fully open (chopper slit directly in front of collimating slit) to fully closed (chopper blocking collimating slit) time of 1.25 μs. At present, the aperture is 10 cm in front of the slit, which is 5 mm from the chopper. The chopped neutrals then stream down the 1.6 m flight tube to the detector, a Magnum 5903 EDR CEM from BURLE Electro-Optics, Inc. (recently acquired by PHOTONIS).

To minimize the uncertainty in energy, the slit width d must also be minimized. A constraint placed on the minimum value of d arises from the disk manufacturing process involved. The disk was photochemically etched out of 130 μm stainless steel, which allows for a minimum value for d of (0.15 ± 0.013) mm. The collimating slit was also chosen with this width to minimize energy uncertainty.

The TOF design is based on a variable chopper rotation frequency between 165 and 500 Hz, where the range was chosen so that the uncertainty $\Delta E/E$, explained in Sec. IV B, is below 0.1 and the rotation frequency does not exceed the limits of the motor. The open:closed duty cycle of the chopper is 0.065, allowing a maximum of ten distribution function samples to be taken over the $\sim$100 μs plasma confinement time at the maximum rotation frequency.

The 50 g stainless steel disk has a 30 g, 1.6 mm thick G-10 support with a 6 cm radius attached to it using cyanoacrylate to allow static balancing of the disk by drilling material out of the G-10. The support allows the disk to be tightened on the collet assembly without damage.

The disk is driven by a MULTIPLEX BL-480/6D brushless RC airplane motor rated at 45 000 maximum rpm (750 Hz). The rotor has four poles composed of neodymium magnets and the stator has six sections of windings. Since the temperature characteristics of these types of motors are not known in vacuum, the temperature was monitored with a thermistor to prevent damage to the Nd magnets caused by overheating due to friction in the bearings and Joule heating in the motor windings. Continuous operation at 165 Hz rotational frequency for over an hour in vacuum results in a temperature rise from 25 to 38 °C, showing that overheating is not an issue.

A He–Ne laser module is mounted inside the vacuum vessel on one side of the chopper and a photodiode is placed on the opposite side. This is used as a reference signal for the slot open time and to monitor the rotation frequency. The arrangement is chosen so that the laser light passes through the same slit as the neutrals to avoid error due to slight disk vibrations. The sensitivity of the positioning of the collimating slit relative to the chopper is 120 μm/μs at the operating rotation frequency. This means that an offset of the collimating slit position relative to the chopper of 120 μm in the direction of rotation corresponds to a timing difference of 1 μs in when the the chopper is open. For this reason one must calibrate this offset each time the slit is moved, as described in Sec. III, in order to use the laser as a timing reference.

Spatial resolution of the diagnostic is determined by the projection of the detector onto the plasma. The CEM has a 7 mm radius resulting in an elliptical projection through the collimating slit with semimajor and semiminor axes of 8 and 4 mm, respectively, due to the divergence of the neutral particle trajectories. The diagnostic is attached to the system vessel by a stainless steel bellows to change the line of sight by pivoting in two dimensions. Adjustable feet allow the detector height to be raised and lowered to change the incident angle between 8.5° and −12° relative to the horizontal. This translates to a radial scan covering the range of 11–26 cm at the midplane. Scans along the horizontal axis are performed by pivoting the whole diagnostic horizontally. Changing the apparatus' incident angle between ±10° translates to a ±10 cm sweep.

B. Electronics

The main electrical components are grouped into three categories: motor control, chopper timing, and particle detection. The motor is controlled by a Castle Creations Thunderbird-18 RC motor controller whose rotation frequency is governed by both a 50 Hz pulse-width-modulated (PWM) signal across its inputs[9] and a 9–20 V dc power source. The duty cycle of the PWM signal varies from 0.05 to 0.1, corresponding to no rotation and the fastest rotation, respectively. Since the motor controller is designed for RC use, the minimum duty cycle of 0.05 from the PWM signal is necessary to emulate the presence of the radio receiver. The controller typically is powered with a 15 V supply and a PWM duty cycle of about 0.07 for a chopper rotation frequency of 165 Hz.

The heart of the chopper timing control is the reference laser, a He–Ne laser module, whose signal is used to generate a square pulse from light passing through the chopper. The reference laser photodiode is an OP906, with a fast ($\sim$5 ns) response time. The photocurrent is converted into a voltage by a 1.5 kΩ resistor, which is then amplified by 150 times using an OPA657 operational amplifier with a gain-bandwidth product of 1600 MHz. The amplified signal is then converted into a transistor-transistor logic (TTL) square pulse through an inverter with Schmitt trigger inputs.

In order to control when the chopper slot first opens, t_{open}, relative to the plasma firing sequence, the delay circuit shown in Fig. 2 has been implemented to trigger the system after receiving a pulse from the reference laser signal. The circuit is armed by a trigger from the machine operator and after the reference signal arrives, an output pulse is sent to a variable delay box used to control t_{open}. The delayed pulse is

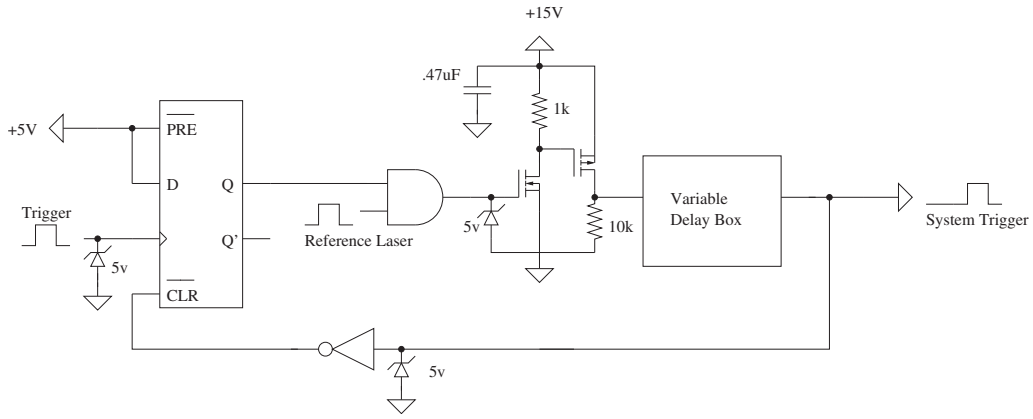

FIG. 2. Synchronization circuit allowing a variable delay between system firing and the initial slit open time.

then used to fire the system, trigger the oscilloscopes, and reset the synchronization circuit allowing t_{open} to be varied from shot to shot.

dc biasing of the detector was accomplished through the use of an UltraVolt, Inc. −4 kV high voltage power supply. For noise reduction, the power supply has a Mu-metal/rf shielded case and an electronic line filter.

The CEM collector output is fed into a 2 kΩ resistor and then into a high bandwidth buffer to drive the 50 Ω cable. Data acquisition is accomplished using a Tektronix TDS 2014 digital storage oscilloscope.

III. REFERENCE LASER CALIBRATION WITH A XENON SOURCE

In order to perform the transformation from the time to velocity (and energy) domain, the time at which the chopper slits pass in front of the collimating slit must be calibrated. The reference laser can be used for this purpose provided that the delay between it and the detector signal is measured. Ultraviolet (UV) light can be used as a source since the channeltron is sensitive to light with wavelengths shorter than ~160 nm.[10] Although it was discovered the IFRC plasma produces enough UV to be used as a timing reference, the diagnostic timing was also verified using a xenon lamp as a UV source, as described here.

A xenon discharge lamp was placed on the opposite side of the vacuum vessel as a UV light source. Since the emission spectra for a typical continuous wave xenon lamp falls below 1% around 200 nm,[11] and the transmittance through the sapphire window is less than 10%, the incident flux in the vacuum UV range was expected to be very small. It was observed that, on the average, there were approximately five photons detected every second. Because of this extremely low count rate, signals were triggered off of the photon signal from the channeltron amplifier circuit and the delay was measured between the photon peak and the reference laser signal.

To account for the finite open time of the chopper, an average of 128 photon triggers was performed using the oscilloscope's averaging feature on the reference laser signal. The expected signal, $F(t)$, was computed numerically by a convolution[12]

$$F(t) = \int_{-\infty}^{\infty} d\tau f(\tau) A(t-\tau), \tag{1}$$

where $A(t)$ represents the cross-sectional area of the opened chopper slit as a function of time,

$$A(t) = \begin{cases} A_{slit}\left(1 - \dfrac{|t|}{t_g}\right) & |t| \leq t_g \\ 0 & |t| > t_g, \end{cases} \tag{2}$$

$f(t)$ is the response of a single pulse from the reference laser, A_{slit} is the area of the chopper slit, 0.76 mm^2, and t_g is half of the total gate time, or 1.25 μs.

An average of five shots, each shot an average of 128 photon triggers, was compared with the numerical convolution to confirm agreement. The time delay between the reference laser and detector signal was then measured to be 1.6 μs.

As discussed in Sec. V, UV light produced in the IFRC can be used as a timing reference. This calibration procedure verified that the observed large peaks (>10% maximum signal) from the IFRC were due to UV light rather than fast neutrals. In experiments where there is no UV light produced, this procedure can be used prior to data collection in the absence of UV light for an absolute timing calibration.

IV. CALIBRATION USING A LITHIUM ION SOURCE

A. Energy scan

An energy calibration of the TOF diagnostic was performed using a lithium ion beam.[13] An ion source with a tunable energy was used to verify that the TOF diagnostic measured the expected energies. The UV calibration method described in Sec. III could not be used as a timing reference for this test, since the ion source blocked the UV photon path. Using a 500 V emitter bias for the source, an energy of 460 eV (obtained from the ion source calibration[13]) was used to calculate the slot open time and an energy scan was performed.

The lithium source produces a beam current of 0.1–1 mA/cm^2, which corresponds to a maximum of 1.8 × 10^{15} ions/s. Taking into account the beam divergence of 3° and the flux reduction due to the slit geometry, the maxi-

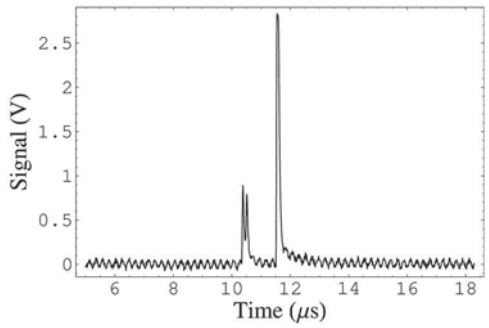

FIG. 3. Shot 2300—pulses from lithium ion source. Emitter bias 800 V, chop frequency 26 kHz. Two neutrals are observed near 10.5 μs and one at 11.5 μs. The amplitude differences are attributed to the pulse height distribution (Ref. 10).

mum expected ion rate was around 9 ions/μs. The measured unchopped ion rate was actually 3 ions/μs for an emitter bias of 600 V, meaning the count rate was low enough to detect individual particles.

The ion source bias voltage was varied over its entire range, 300–1500 V, and five shots were taken for each bias as an energy scan. Because of the low ion flux, only one to five ions were typically detected per 2.5 μs gate time. A sample shot is shown in Fig. 3. For all data used in this section, the oscilloscope was triggered off of the TTL signal generated from the reference laser and the pulse times were all measured from the point at which the signal was 5% of the maximum on the leading edge.

For the data shown in Fig. 4, the delay between the reference laser and the average pulse position, Δt_{total}, was measured for a 500 V emitter bias on the ion source. The delay between the slot open time and the reference laser signal, Δt_{ref}, was then calculated using an average ion energy of 460 eV

$$\Delta t_{\text{ref}} = \Delta t_{\text{total}} - \Delta t_{460}, \tag{3}$$

where Δt_{460} is the travel time for a 460 eV Li ion, which is 14.2 μs for a 1.6 m distance. Δt_{ref} was then used to calculate the slot open time for various ion energies as the emitter bias was scanned. The standard deviation of the 500 V bias data was 1.06 μs and can be attributed to the finite slit open time.

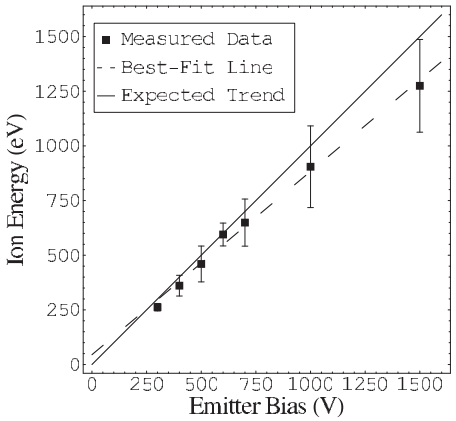

FIG. 4. Lithium ion energy scan. Expected trend (solid) represents a 1:1 correspondence between ion energy and emitter bias. Best-fit line (dashed) falls within error bars.

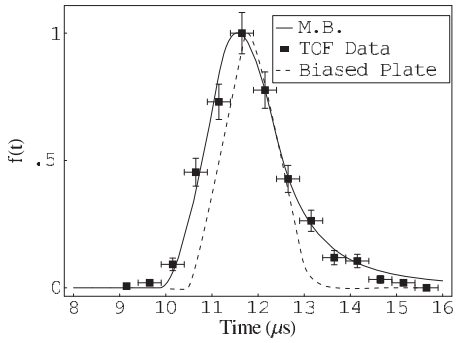

FIG. 5. Lithium ion distribution function for 800 V bias in time domain as measured by TOF diagnostic (boxes) where data are binned into 500 ns intervals. The Maxwell–Boltzman distribution comparison (solid) with 83 eV temperature and 750 eV drift convoluted with the aperture function and compared to convoluted biased plate collector data (dashed) from the ion beam calibration (Ref. 13).

Error bars in Fig. 4 were calculated by the deviation from the mean at each bias voltage. As shown, the fitted line of the averaged data differs from the expected energies by 16%.

B. Lithium energy distribution function

To determine the distribution function, 650 pulses were sampled at an 800 V emitter bias and binned according to the time difference between the reference laser and the arrival time, as shown in Fig. 5. The flux from a drifting Maxwell–Boltzman distribution with a peak energy of 750 eV and temperature of 83 eV (computed by a least-squares fit) is shown in addition to data taken from a biased planar collector.[13] The Maxwell–Boltzman distribution and the collector data have both been transformed to the time domain and convoluted with the aperture function, Eq. (2), in order to compare with the TOF data. Since the data consist of a finite number of points, the convolution performed was a discretized form of Eq. (1).

The emitter temperature in the ion source is typically 1100 °C, or 0.1 eV. Since the TOF data show a broadening of 83 eV at a 750 eV beam energy, the resulting uncertainty, $\Delta E/E$, is 0.11. The theoretical uncertainty, $\Delta E/E$, is 0.09 and is computed by

$$\frac{\Delta E}{E} = \frac{E(v) - E\left(\dfrac{L}{L/v + t'}\right)}{E(v)}, \tag{4}$$

where $E(v)$ is the energy for a velocity v, $L/(L/v+t')$ is the shift in velocity resulting from the finite open time of the chopper, and $t'=0.5$ μs, obtained by integrating the aperture function, is the time at which all but e^{-1} of the transmitted particles pass through the chopper.

V. PERFORMANCE IN THE FRC

TOF data from the FRC are shown in Fig. 6. Timing calibration described in Sec. III was performed to verify that the peaks at 37 and 75 μs are photon pulses from emitted UV radiation. In all further data analysis, the photon peak is used as a timing reference. It should be noted that as the detector bias increases, the photon pulse distorts and widens due to saturation of the detector. This explains why the pho-

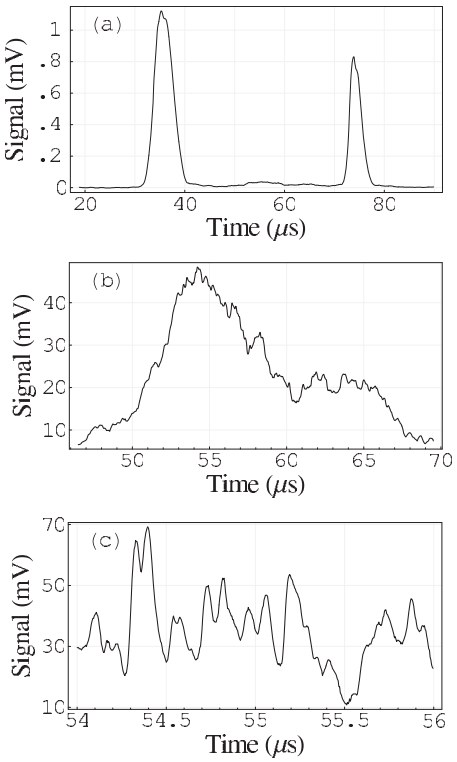

FIG. 6. TOF data from IFRC for CEM biased at −2.5 kV. The data have been smoothed over 1 μs for (a) and (b). The photon peaks are shown in (a), while the neutral signal in (b) has been zoomed to show response from individual ions in (c).

ton peak in Fig. 6(a) is wider than the 2.5 μs slot open time. At low bias voltages (~1.5 kV), however, the photon peak closely resembles the expected aperture function from Eq. (2). To verify that the detector has recovered from saturation, the output current has been integrated to show that the total charge depletion is typically less than 10% of the total charge, indicating there is still plenty of charge reserved for when the neutrals arrive.

The charge-exchanged neutral signal lies between the photon pulses and can be seen by increasing the vertical resolution, as shown in Fig. 6. The data indicate that the neutral detection is operating in a regime between analog and pulse counting mode, as seen by the sharp pulses overlaid on top of a broad signal.

Since the slit open time has a finite width, the distribution function is broadened due to particles with different energies leaving the slit at different times. As described in Sec. III, the resulting signal is the convolution between the aperture function and the signal for a delta function aperture. The theoretical uncertainty in energy, $\Delta E/E$, due to this is around 0.04 in the observed energy range, as calculated by Eq. (4).

To arrive at the distribution function, $f(E)$, the data must first be transformed from the time domain into velocity space by the replacement

$$f(t) \rightarrow f\left(\frac{L}{t-t_0}\right), \tag{5}$$

where L is the flight distance, 1.6 m, and t_0 is the open time of the slit, measured from the UV photon pulse. The velocity, v, is then converted into its corresponding energy for a hydrogen atom.

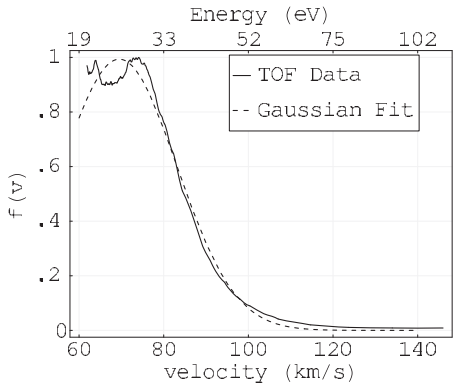

FIG. 7. Ion distribution function measured by TOF diagnostic compared to a Gaussian fit.

The data must also be corrected for detector sensitivity and charge-exchange cross-sectional dependence on particle energy. For atomic hydrogen, the charge-exchange cross section is empirically[14]

$$\sigma(E) = (7.6 \times 10^{-8} - 1.06 \times 10^{-8} \log_{10} E)^2 \text{ cm}^2. \tag{6}$$

Over the relevant energy range, the relative correction for charge-exchange cross section between the low and high energy is roughly 15%. The detector sensitivity, however, has a much greater effect. Calibration for microchannel plates has been performed down to 20 eV,[7] and the sensitivity is linear in this range. Correction for these results in the distribution function shown in Fig. 7. To smooth out the individual pulse data, the data shown are averages of four shots with the same charging and timing parameters and have been smoothed over 1 μs. A Gaussian fit which closely matches the observed distribution is shown in the dashed trace with a 25 eV drift velocity and 2 eV temperature.

[1] D. E. Voss and S. A. Cohen, Rev. Sci. Instrum. **53**, 1696 (1982).
[2] H. Verbeek, J. Phys. E **19**, 964 (1986).
[3] R. L. Boivin, M. Koltonyuk, C. P. Munson, and R. M. Mayo, Rev. Sci. Instrum. **68**, 982 (1997).
[4] N. R. Ray, J. Phys. D: Appl. Phys. **31**, 1071 (1998).
[5] Z. A. Pietrzyk, G. C. Vlases, R. D. Brooks, K. D. Hahn, and R. Raman, Nucl. Fusion **27**, 1478 (1987).
[6] I. L. Kofsky and H. Levinstein, Phys. Rev. **74**, 500 (1948).
[7] B. L. Peko and T. M. Stephen, Nucl. Instrum. Methods Phys. Res. B **171**, 597 (2000).
[8] D. E. Voss and S. A. Cohen, J. Vac. Sci. Technol. **17**, 303 (1980).
[9] T. van Roon, Servo Pulser (http://www.uoguelph.ca/antoon/gadgets/servo3.htm).
[10] Channeltron Electron Multiplier Handbook for Mass Spectrometry Applications, Galileo Electro-Optics, 1991.
[11] R. A. Capobianco, "Xenon: The full spectrum vs. deuterium plus tungsten," PerkinElmer, Inc. Application Notes.
[12] J. A. Alcalay and E. L. Knuth, Rev. Sci. Instrum. **40**, 438 (1969).
[13] Y. Zhang, H. Boehmer, W. W. Heidbrink, R. McWilliams, D. Leneman, and S. Vincena, Rev. Sci. Instrum. **78**, 013302 (2007).
[14] W. L. Fite, A. C. H. Smith, and R. F. Stebbings, Proc. R. Soc. London, Ser. A **268**, 527 (1962).